PNAS RESEARCH ARTICLE | BIOPHYSICS AND COMPUTATIONAL BIOLOGY
MICROBIOLOGY

Active interface bulging in *Bacillus subtilis* swarms promotes self-assembly and biofilm formation

Siyu Liu[a,1], Ye Li[a,b,1], Haoran Xu[a,2], Daniel B. Kearns[c], and Yilin Wu[a,3]

Edited by Ned S. Wingreen, Princeton University, Princeton, NJ; received December 14, 2023; accepted June 21, 2024 by Editorial Board Member E P. Greenberg

Microbial communities such as biofilms are commonly found at interfaces. However, it is unclear how the physical environment of interfaces may contribute to the development and behavior of surface-associated microbial communities. Combining multimode imaging, single-cell tracking, and numerical simulations, here, we found that activity-induced interface bulging promotes colony biofilm formation in *Bacillus subtilis* swarms presumably via segregation and enrichment of sessile cells in the bulging area. Specifically, the diffusivity of passive particles is ~50% lower inside the bulging area than elsewhere, which enables a diffusion-trapping mechanism for self-assembly and may account for the enrichment of sessile cells. We also uncovered a quasilinear relation between cell speed and surface-packing density that underlies the process of active interface bulging. Guided by the speed–density relation, we demonstrated reversible formation of liquid bulges by manipulating the speed and local density of cells with light. Over the course of development, the active bulges turned into striped biofilm structures, which eventually give rise to a large-scale ridge pattern. Our findings reveal a unique physical mechanism of biofilm formation at air–solid interface, which is pertinent to engineering living materials and directed self-assembly in active fluids.

biological active matter | bacterial swarm | biofilm | active Brownian particle model | self-assembly

Significance

Microbial communities of ecological and clinical importance are commonly found in interface-associated environments. The physical environment of interfaces may contribute to the development and behavior of surface-associated microbial communities. Here, we find that an actively expanding *Bacillus subtilis* colony grown at air–solid interface can spontaneously develop interface bulges; the bulging areas tend to enrich immotile cells via a diffusion-trapping mechanism and thus have a higher propensity to transit into a biofilm state. Our findings demonstrate the important role of active interfacial mechanics in bacterial collective behavior, providing a unique approach for colony biofilm patterning and directed self-assembly.

Microbial communities of ecological and clinical importance are commonly found in interface-associated environments, such as biofilms (1, 2) and bacterial swarms (3, 4) on solid substrates, pellicles at liquid–air interface (5), and microbiomes thriving in the gastrological tract of animals (6). Mechanical forces at the interfaces are expected to play crucial roles in the surface-associated life of microbial communities (7–11). For instance, cell–substrate mechanical interaction drives biofilm morphogenesis and orientational ordering of cells (12, 13), while surface flows have been shown to promote the expansion (14–19) and material transport (20) within bacterial colonies. However, it remains largely unexplored how the physical environment of interfaces may contribute to more diverse processes involved in the development and behavior of surface-associated microbial communities.

Here, we focus on the transition between the motile and sessile state of bacterial communities grown on solid substrates, a key step in the adaptation to environmental fluctuations of bacterial communities (9, 21, 22). During the transition, cells switch their gene regulation program from expressing flagellar genes to one that expresses biofilm genes and deactivates flagellar motility (23, 24). The transition generally requires surface-sensing mediated by cell surface appendages (25–27) or envelope stress (28, 29) but can also be facilitated by purely physical mechanisms such as motility-induced phase separation (MIPS) and motility segregation (30, 31).

In this study, we find that an interfacial process denoted as "active interface bulging" promotes the transition from motile-to-sessile biofilm state of *Bacillus subtilis* communities at air–solid interface. During the process, an initially two-dimensional (2D) layer of swarming motile cells spontaneously develops scattered liquid bulges at the free-surface of swarm fluid film manifesting as regions where cells are highly motile and can pile on top of one another. The bulges have a higher propensity to transit into sessile colony biofilm state; using experiments and active Brownian particle simulations, we attribute this result to the enrichment of sessile cells toward the bulging area driven by a diffusion-trapping mechanism. We also found that a quasilinear relation between cell speed and surface-packing density underlies liquid bulge formation; this relation informs the control of active bulging process. Our findings illustrate the importance of interfacial mechanics to a comprehensive understanding of bacterial behavior and dynamics. The findings are also pertinent to biofilm patterning in engineered living materials (32–34) and directed self-assembly in active matter fluids (35–38).

Author affiliations: [a]Department of Physics and Shenzhen Research Institute, The Chinese University of Hong Kong, Shatin, NT, Hong Kong, People's Republic of China; [b]Shenzhen Institute of Synthetic Biology, Shenzhen Institutes of Advanced Technology, Chinese Academy of Sciences, Shenzhen, Guangdong 518055, China; and [c]Department of Biology, Indiana University, Bloomington, IN 47405-7005

Author contributions: S.L., Y.L., D.B.K., and Y.W. designed research; S.L., Y.L., and H.X. performed research; D.B.K. and Y.W. contributed new reagents/analytic tools; S.L., Y.L., and Y.W. analyzed data; and Y.W. wrote the paper.

The authors declare no competing interest.

This article is a PNAS Direct Submission. N.S.W. is a guest editor invited by the Editorial Board.

[1]S.L. and Y.L. contributed equally to this work.

[2]Present Address: Institute for Advanced Study in Physics, Zhejiang University, Hangzhou 310027, China.

[3]To whom correspondence may be addressed. Email: ylwu@cuhk.edu.hk.

This article contains supporting information online at https://www.pnas.org/lookup/suppl/doi:10.1073/pnas.2322025121/-/DCSupplemental.

Published July 25, 2024.

Results

Liquid Bulges Spontaneously Emerge in Homogeneous *B. subtilis* Swarms. To study motile-to-sessile state transition in surface-associated bacterial communities, we chose to work with bacterial swarms (3, 4). Bacterial swarming resembles the early stage of colony biofilm formation on solid substrates (21), during which bacterial colonies extract liquid from the surroundings to form a free-surface liquid film that covers the entire colony and supports flagellar motility (39, 40). *B. subtilis* is a model microorganism that displays robust swarming behavior (4). When *B. subtilis* swarms were grown on agar surface with intermediate wetness, we found that an initially homogeneous 2D monolayer of motile cells in *B. subtilis* (wild-type NCIB3610) swarms can spontaneously develop a temporally stable pattern of scattered domains (Fig. 1*A*, *Methods*, and Movie S1) with higher surface-packing density of cells (Fig. 1*B* and *Methods*); here, surface-packing density refers to the number of cells in the swarm sitting above unit area of agar surface. The boundaries of such domains are dynamic but well-defined in low magnification phase-contrast images (Fig. 1*A*) or in darkfield microscopy images (Fig. 1*B*). In contrast to cells moving in a strictly 2D manner (i.e., as a monolayer) outside these domains, cells inside the high-surface-density domains often overlap with each other (Movie S2), showing that the height of swarm fluid film in these domains is greater than that in the monolayered regions. Moreover, cells within the high-surface-density domains move freely with the mean speed and persistence time (i.e., the time during which a cell does not substantially change the moving direction; *SI Appendix*) only slightly lower (~7% for mean speed and ~9% for persistence time) than elsewhere (Fig. 1 *C* and *D* and *Methods*), which is different from the clustering domains formed in *B. subtilis* swarms via MIPS (30, 41) that consist largely of jammed cells. The similar mean speed and persistence time suggests that the volume density of cells is nearly homogeneous throughout the swarm fluid film. Therefore, the high-surface-density domains are in fact

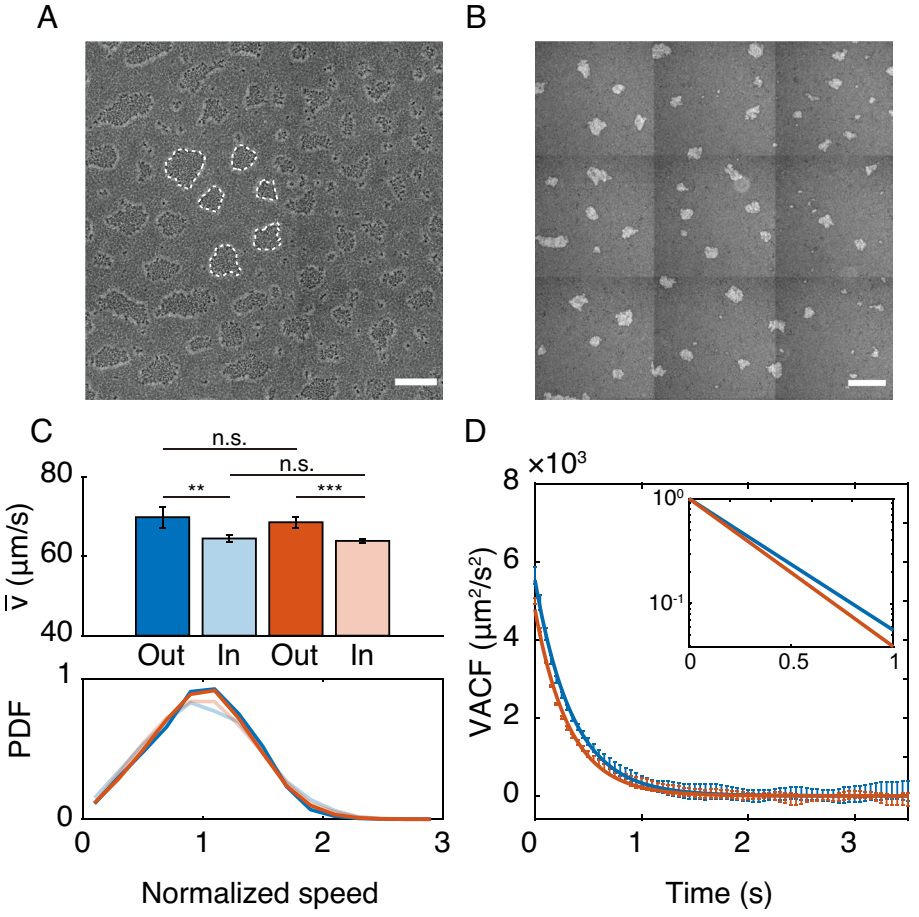

Fig. 1. Liquid bulges with higher surface-packing cell density emerge in *B. subtilis* swarms. (*A*) A representative large-field phase-contrast microscopy image (*Methods*) showing a pattern of scattered domains in the swarming colonies of *B. subtilis*. Dash lines indicate the boundaries of such domains. (*B*) A representative large-field darkfield microscopy image of the scattered-domain pattern similar to that shown in panel *A* (*Methods*). In darkfield microscopy, the brightness is positively correlated with surface-packing density of cells, thus brighter domains in the image have higher surface-packing cell density. Panels *A* and *B* were obtained by stitching overlapping images taken in a smaller field of view. (Scale bar in panels *A* and *B*, 500 μm.) (*C*) Motion pattern of cells inside and outside the high-surface-density domains (or liquid bulges) when stable liquid bulges were just formed. (*Upper*) Average speed ($-v$) of cells that crossed the boundaries of the domains during the tacking period are shown as columns in dark blue (outside the domains; 69.8 ± 2.6 μm/s, mean ± SE, N = 4) and light blue (inside the domains; 64.5 ± 0.9 μm/s, mean ± SE, N = 4), respectively; average speed of cells that remained outside and inside the high-surface-density domains during the single-cell tracking period are shown as columns in dark red (68.5 ± 1.3 μm/s; mean ± SE, N = 5) and light red (63.8 ± 0.5 μm/s; mean ± SE, N = 5), respectively. Statistical analysis was performed using Welch's two-tailed *t* test: n.s., not significant; $^{**}P < 0.01$; $^{***}P < 0.001$. Exact *P* values from *Top* to *Bottom*: 0.3697, 0.2257, 0.0080, and 7.6×10^{-5}. (*Lower*) Average probability density functions (PDFs) of the normalized speed of cells corresponding to the four scenarios in the *Upper* panel, following the same color coding as that of the columns in *Upper* panel. The speed was normalized by the mean speed of all cells in the corresponding scenario. (*D*) Velocity autocorrelation functions (VACFs) of cells that remained inside and outside the liquid bulges computed based on single-cell trajectories. Solid lines are exponential fits to the VACFs (blue: outside liquid bulges, $\mathrm{VACF}_{out} \sim \exp(-t/0.35)$, persistence time $\tau_{out} = 0.35 \pm 0.01$ s; red: inside liquid bulges, $\mathrm{VACF}_{in} \sim \exp(-t/0.31)$, persistence time $\tau_{in} = 0.31 \pm 0.01$ s). The diffusivity computed from VACF is ~20% lower inside bulges than outside (~980 $\mu m^2/s$ vs. ~770 $\mu m^2/s$) (*Methods*). Plotted in the inset are normalized fitted VACFs outside (blue) and inside (red) liquid bulges in semilogarithmic scale. Error bars represent the SD of N = 5 biological replicates.

bulges of the swarm fluid film at its free-surface, where more motile cells can be accommodated per unit surface area due to the greater fluid height. We noted that the wetness of agar surface is a key factor for producing the liquid bulges (*SI Appendix, SI Methods*).

To examine whether cells inside and outside the liquid bulges represent different subpopulations with intrinsic motility difference, we tracked the motion of cells near the bulge boundaries. We found that cells can freely cross the boundary (Movie S2); the same cell had a slightly lower mean speed inside bulges than outside the bulges (Fig. 1*C*, blue columns in the *Upper*), with magnitudes similar to those that had not crossed the boundaries during the period of tracking. In other words, when cells entered the liquid bulges, their speed decreased slightly and vice versa. Moreover, the probability density functions of normalized bacterial speed inside and outside liquid bulges are similar (Fig. 1 *C*, *Lower*). These results together show that the speed difference inside and outside liquid bulges is not due to the presence of subpopulations with intrinsic motility difference. One interpretation of this finding is that the local physical environment inside liquid bulges is different from outside.

Nonetheless, immotile cells with deactivated flagellar motility can naturally arise in a swarm due to cell–cell variability of motility (42, 43) or due to the genetic program of motile-to-sessile transition (23, 44–46), and a recent study suggests that immotile subpopulation nucleates stationary clusters in *B. subtilis* swarms (31). To examine whether immotile cells in the swarm contribute to liquid bulge formation, we chose a Δ*sinI* mutant of *B. subtilis*, which is incapable of differentiation into sessile cells and thus retains active flagellar motility (47, 48). We found a similar phenomenon of liquid bulge formation in swarms of *B. subtilis* Δ*sinI* mutant (Movie S3), and cells inside and outside the liquid bulges displayed similar motion patterns compared to their counterparts in wild-type *B. subtilis* swarms (*SI Appendix*, Fig. S1). These results show that liquid bulge formation does not require an immotile subpopulation of cells in the swarm. Taken together, the liquid bulges we report here are different from those patterns of scattered domains found in bacterial colonies whose formation is driven by MIPS (30, 41) or by nucleation of immotile cells (31) (*Discussion*).

Liquid Bulges Have a Higher Propensity to Transit Into Biofilm State. Within ~20 to 30 min after the emergence of stable liquid bulges, the liquid bulges grew in size and passively slid along the colony expansion direction; meanwhile, nearby bulges along the colony expansion direction coalesced and fused into stripes (Fig. 2*A* and Movie S1). For wild-type swarms, cells outside the striped bulges remained highly motile, but the motility of cells inside the bulges gradually decreased (Fig. 2*B*). After ~2 to 3 h from the formation of striped liquid bulges, most cells in the bulges became immotile and cells appeared to have a chained-like

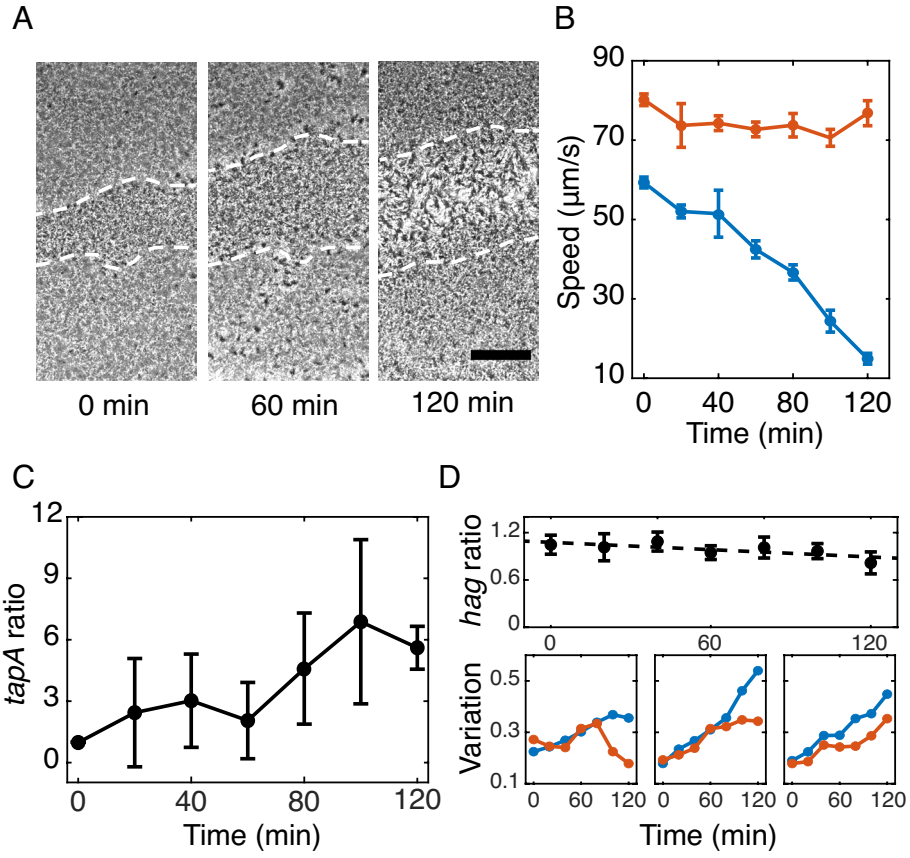

Fig. 2. Transition of cells in bulges into biofilm state. (*A*) Phase-contrast microscopy image sequence showing the development of liquid bulges in a wild-type swarm. Striped liquid bulges are shown as patterns in between the dashed lines at the center of images along the horizontal direction with different contrast. (Scale bar, 300 μm.) In all other panels T = 0 min corresponds to the state shown in the *Left* image of panel *A*, i.e., shortly after stable liquid bulges had developed into striped patterns. (*B*) Temporal dynamics of average collective speed of cells inside (blue) and outside (red) liquid bulges in a wild-type swarm computed by optical flow analysis (*Methods*). Error bars represent SD of collective speed distributions in the two regions. The speed decrease inside bulges shown in Fig. 2*B* is due to progressive enrichment and proliferation of immotile cells in the bulges. (*C*) Temporal dynamics of the ratio between average single-cell P_{tapA}-*gfp* reporter activity inside and outside liquid bulges. Error bars represent SD (N = 3). (*D*) Temporal dynamics of single-cell P_{hag}-*gfp* reporter activity. (*Upper*) The ratio between average single-cell P_{hag}-*gfp* reporter activity inside and outside liquid bulges plotted against time (indicated in the abscissa). Dash line is a least-squares linear fit with slope ~−0.0015 (R^2 = 0.58). Error bars represent SD (N = 4). (*Lower*) Normalized spatial variation of the P_{hag}-*gfp* reporter fluorescence inside (blue) and outside (red) bulges (*Methods*); data in each panel are from one representative experiment and the dynamics show variability across experiments. Solid lines in panels *B*–*D* serve as guides to the eye.

morphology characteristic of cells in *B. subtilis* biofilms (5) (Fig. 2 *A*, *Right* and Movie S4); intriguingly, a large-scale pattern of parallel ridges with high cell densities eventually emerged in between the striped biofilm structures, suggesting a unique route to biofilm maturation other than wrinkling (*Discussion*). By contrast, in swarms of the Δ*sinI* mutant, cells did not chain and remained highly motile everywhere as liquid bulges continued to merge with each other; eventually, liquid bulges covered the entire field of view (Movie S3), at which time the swarm became homogeneous again. These observations suggest that liquid bulges of wild-type swarms have a higher propensity than elsewhere to transit from motile-to-sessile or biofilm state. To examine this idea, we monitored the physiological state of wild-type cells inside and outside liquid bulges with four fluorescent reporters starting from the emergence of stable liquid bulges (*Methods*): P_{tapA}-*gfp* and P_{epsA}-*gfp*, genetically encoded fluorescent reporters for the gene expression level of *tapA* (encoding an anchor protein TapA for biofilm matrix component TasA) and of *epsA* (encoding the biofilm matrix component exopolysaccharide) (49–52), both of which have served as indicators of biofilm formation (53–56); P_{hag}-*gfp,* a genetically encoded fluorescent reporter for the expression level of *hag* gene (encoding flagellin protein) serving as an indicator of cell motility (42, 49); and the lipophilic dye FM4-64 that stains the cell membrane and indicates cell density (57). The fluorescence of FM4-64 allows us to perform density correction on the total fluorescence counts of the gene reporters, so that we can measure single-celled gene reporter activities in a manner insensitive to cell density variation (*Methods*).

We found that the ratio between single-cell P_{tapA}-*gfp* reporter activities inside and outside liquid bulges gradually increased throughout the developmental process (Fig. 2*C*). Meanwhile, although single-cell P_{epsA}-*gfp* reporter activity could not be monitored continuously over time due to the low fluorescence intensity of this reporter, we found that it was higher inside the bulges than outside at the later stage of bulge development (*SI Appendix*, Fig. S2). The consistency in the temporal dynamics of the activities of both biofilm matrix reporters shows that the liquid bulges have a higher propensity to transit into a colony biofilm state. On the other hand, the ratio between single-cell P_{hag}-*gfp* reporter activities inside and outside liquid bulges showed no significant decrease throughout the developmental process (Fig. 2 *D*, *Upper*). This result is unexpected, because the expression levels of *tapA* and *hag* are supposed to be inversely correlated (49) and thus one would expect a substantial decrease in the ratio of P_{hag}-*gfp* reporter activities. However, close inspection of the fluorescence images revealed that the striped liquid bulges displayed larger spatial variation of the P_{hag}-*gfp* reporter fluorescence after ~80 min from their formation (Fig. 2 *D*, *Lower*), with randomly spaced cellular clusters of much higher P_{hag}-*gfp* reporter fluorescence than elsewhere (*SI Appendix*, Fig. S3); the brighter fluorescence from these clusters masked the reduced P_{hag}-*gfp* reporter activity of chained cells inside liquid bulges. Cellular clusters with high P_{hag}-*gfp* reporter fluorescence likely arose from stochastic switching from chained to motile state (45, 46), and they appeared immobile because of jamming or entrapment in between the chained cells. Overall, the reporter results show that liquid bulges of wild-type swarms indeed are more prone to transiting into the biofilm state. Thus, the formation of liquid bulges represents an unrecognized biophysical mechanism that promotes biofilm formation at air–solid interface; it is distinct from mechanisms mediated by MIPS (30) or by nucleation of immotile cells (31).

Liquid Bulge Formation Depends on Cell Motility and Density. Next, we sought to understand how the liquid bulges form and why the bulges are more prone to biofilm transition. To address the first question, we followed the developmental process of the liquid bulges in *B. subtilis* swarms. We found that the formation of liquid bulges was preceded by the spontaneous nucleation of transient domains with high surface-packing density of cells with various sizes of ~10 to 60 μm and ~1 to 2 s lifetime (Movie S5). Within several minutes, the transient domains grew in size and gradually stabilized into liquid bulges with well-defined boundaries. The results indicate that the formation of liquid bulges is associated with transient increase in surface-packing density of cells due to motility-driven density fluctuations in the swarm; such nonequilibrium density fluctuations require local free-energy input and are often seen in quasi-2D self-propelled particle systems at high densities (58–60).

To understand how cell motility and local cell density variation relate to the formation of liquid bulges, we manipulated cell motility in situ in the swarm; here, the nonchaining Δ*sinI* mutant was used in order to exclude the artifact in speed measurement brought by any pre-existing immotile cells. Violet light illumination (~406 nm) was used to reversibly control cell speed because violet light generates reactive oxygen species that suppress flagellar motility (61) (*Methods* and *SI Appendix*, Fig. S4). When we illuminated a region with pre-existing liquid bulges (Fig. 3*A* and Movie S6), cell speed decreased from ~65 μm/s to ~22 μm/s under violet light illumination, and the local cell number density fluctuation $\Delta N/N$ (*Methods*) in the illuminated monolayered regions was decreased; meanwhile, the existing liquid bulge gradually dispersed. Withdrawal of violet light illumination allowed the recovery of cell speed up to ~45 μm/s as well as the recovery of cell density fluctuation, while new liquid bulges emerged (Fig. 3*A*). The result shown in Fig. 3*A* demonstrated that the degree of local cell density fluctuation is strongly correlated with bulge formation.

A Negative Quasilinear Relation between Cell Speed and Surface-Packing Density Underlies Liquid Bulge Formation. In the experiment shown in Fig. 3*A*, the average surface-packing density of cells in the illuminated monolayered regions was increased by a magnitude of ~10% (*SI Appendix*, Fig. S5). This violet light-induced cell density increase is presumably due to reduced cellular flux out of the illuminated area during speed decrease, a phenomenon predicted in self-propelled particles (62) and observed in active bacterial suspensions (30, 37, 38, 63). The magnitude of violet light–induced cell density increase is close to the level of cell density fluctuations at normal speed (~10%; Fig. 3*A*), and it is significant compared to the maximal transient increase of local cell density (~20%) due to the fluctuations. Why wouldn't the violet light–induced cell density increase compensate for the decreased level of local cell density fluctuation and thus prevent the dispersal of liquid bulges during cell speed reduction?

This question prompted us to investigate the detailed relation between cell motility and surface-packing density of cells inside and outside liquid bulges; for both monolayered regions and liquid bulges, surface-packing density is defined as the number of cells in the swarm sitting above unit area of agar surface. For this purpose, we designed a multimode imaging system that integrates large-scale (~3 cm^2) blue/violet light illumination (for speed reduction in the swarm), darkfield microscopy (for speed measurement by optical flow analysis), and wide-field fluorescence microscopy (for surface-packing density measurement by counting the number of fluorescently labeled nonchaining cells) (*Methods* and *SI Appendix*, Fig. S6). Using this multimode imaging system, we found that the surface-packing density of cells showed a negative quasilinear relation with cell speed during bulge formation (Fig. 3*B*). Remarkably, the ratio between surface-packing densities (i.e., cell number per unit surface area but not per fluid volume)

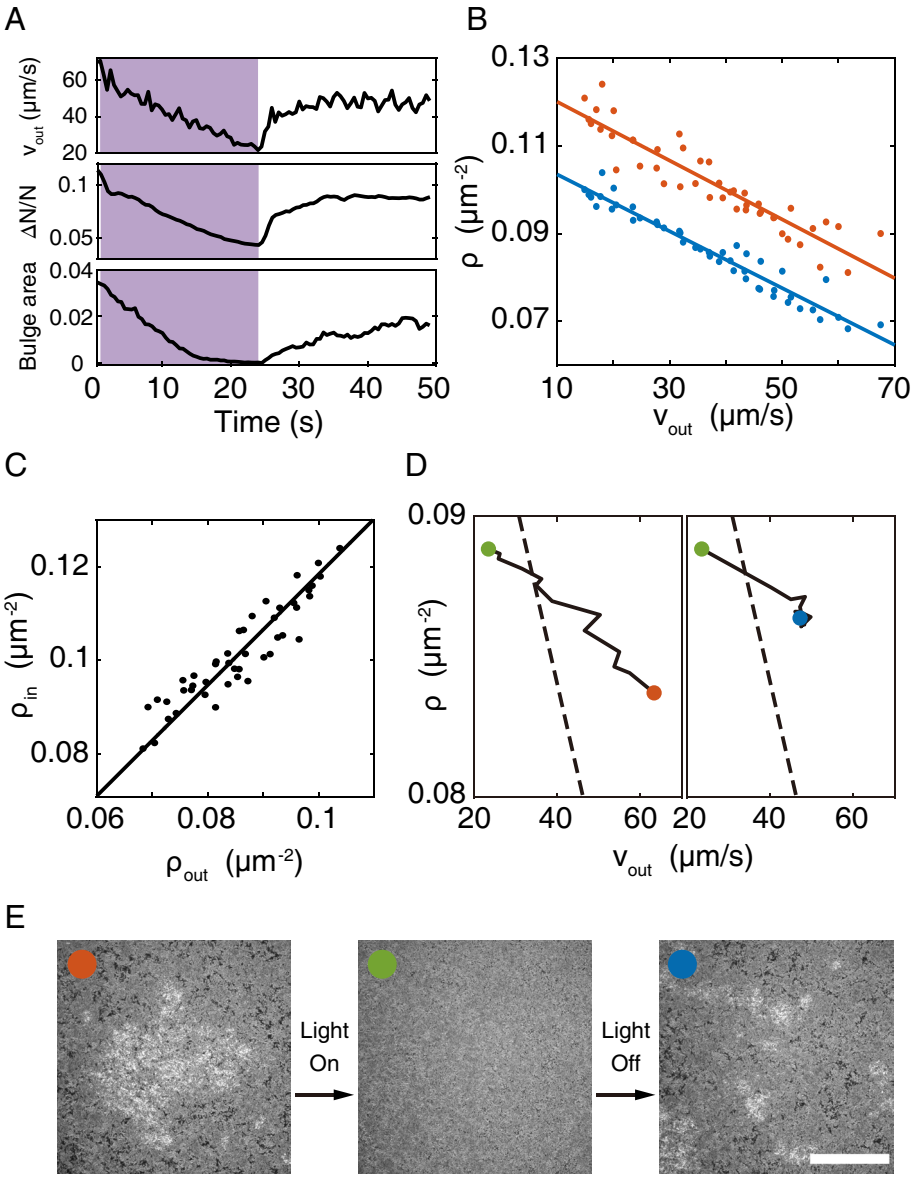

Fig. 3. Motility and density dependence of bulge formation in *B. subtilis* swarms. (*A*) Local cell density fluctuation is correlated with liquid bulge formation. Plotted here are temporal dynamics of collective cell speed outside bulges obtained by optical flow analysis on darkfield microscopy images (v_{out}; *Upper*), cell density fluctuation ($\Delta N/N$, where ΔN and N are the SD and average of cell number, respectively; *Middle*), and area fraction of bulges (*Lower*); see *Methods*. Violet light was illuminated during the period shaded in purple color. (*B*) Relation between cell speed and surface-packing cell number density for monolayered regions (blue) and for the coexisting liquid bulges (red) (*Methods*). Collective cell speed measured in the monolayered regions (v_{out}; *Methods*) was used in the abscissa. Lines are least-squares linear fits to the data (R^2 = 0.94 for blue line and 0.85 for red line). Data presented here was from three biological replicates. (*C*) Relation between surface-packing cell density inside (ρ_{in}) and outside (ρ_{out}) bulges. Solid line is least-squares linear fit with ρ_{in} = 1.18 ρ_{out} (R^2 = 0.83). Data presented here was from three biological replicates. (*D*) Phase trajectories in the plane of cell speed and density during reversible manipulation of the liquid bulge formation in panel *A* (Movie S6). In the phase trajectories, red dot represents the initial state at the beginning of violet light illumination when liquid bulges were present (Time = 0.3 s); green dot represents the state at the end of violet light illumination, at which time liquid bulges had completely dispersed (Time = 24.3 s); blue dot represents the state when bulges re-formed due to motility recovery (Time = 49.8 s). Dash lines are a portion of the blue line in panel *B* (i.e., the fitted speed–density relation for monolayered regions that coexist with liquid bulges). (*E*) Darkfield microscopy images corresponding to the three color-labeled points of the phase trajectories in panel *D*. The brightness in these grayscale images is proportional to surface-packing density of cells, thus brighter domains in the images represent the liquid bulges. (Scale bar, 300 μm.)

inside and outside liquid bulges remained nearly constant at ~1.2 regardless of the cell speed (Fig. 3 *B* and *C*).

To interpret the quasilinear speed–density relation, we note that liquid bulge formation increases interfacial energy of the swarm fluid film, which can be fueled by local increase of activity-induced pressure (i.e., the force exerted on the fluid interface per unit area due to cell motility); see a scaling analysis in *Methods*. As the activity-induced pressure is dependent on both cell speed and surface-packing density, we reasoned that the speed–density relation measured in monolayered regions coexisting with liquid bulges (blue line in Fig. 3*B*) represents the cell speed (or cell density) threshold for bulge formation at a specific density (or speed); above the threshold, the local activity-induced pressure would be sufficiently high to support the formation of stable liquid bulges. According to this notion, either increasing cell speed or increasing cell density in a swarm monolayer could promote the formation of liquid bulges. Indeed, the experiment in Fig. 3*A* corresponds to a case that the cell speed crossed this threshold to a lower level that does not support bulge formation (Fig. 3 *D*, *Left* panel; from red to green point), followed by a speed increase that crossed the threshold again and recovered bulge

formation (Fig. 3 *D*, *Right* panel; from green to blue point). Furthermore, we found that de novo bulge formation can be initiated by increasing the surface-packing density of cells in a monolayered region without bulges while decreasing cell speed (*SI Appendix*, Fig. S7 and Movie S7). The motion pattern of cells inside and outside bulges formed this way was similar to that associated with naturally developed liquid bulges (*SI Appendix*, Fig. S8). These results support the notion that the speed–density relation measured in monolayered regions sets the motility or density threshold for liquid bulge formation. They also demonstrate the feasibility of reversible manipulation of self-assembled liquid bulges in bacterial swarms guided by the quantitative insight from the speed–density relation.

Expedited Biofilm Formation in Bulging Areas Results from the Enrichment of Immotile Cells. Having elucidated the driving factors of bulge formation, we next sought to understand why liquid bulges are more prone to biofilm transition. Immotile cells with deactivated flagellar motility naturally arise in a swarm due to cell–cell variability of motility (42, 43) or due to the genetic program of motile-to-sessile transition (23, 24, 45, 46). With ~20% higher surface-packing cell density, liquid bulges are expected to contain higher surface density of pre-existing immotile cells that have naturally arisen in a swarm; could this fact account for the higher propensity of biofilm transition in the bulging areas? To address this question, ideally, we would need to track the population distribution of immotile cells inside and outside liquid bulges. However, we lack appropriate reporters of immotile cells that are sufficiently bright for single-cell tracking or population density quantification in swarms (note that the biofilm state reporters P_{tapA}-*gfp* and P_{epsA}-*gfp* we used above are very dim and can only detect chained cells that are already in a biofilm state). Instead, we use passive microspheres of a size comparable to cells (diameter ~1 μm) to imitate immotile cells in the swarm and track the motion and spatial distribution of these microspheres (*Methods*).

We deposited passive microspheres in a lawn of the swarm prior to liquid bulge formation and then followed the position of these microspheres when liquid bulges emerged. Unexpectedly, we found that the density of passive microspheres inside liquid bulges kept increasing (Fig. 4*A*, red line; Movie S8); meanwhile, the density outside liquid bulges was slowly decreasing (Fig. 4*A*, blue line). This result shows that the ratio between microsphere densities inside and outside bulges is not constant but keeps increasing, which is in stark contrast to the constant ratio of overall surface-packing densities of cells. To explain the enrichment of passive microspheres inside the bulges, we measured the mean speed of microspheres and found that the speed inside bulges is ~20% lower than outside (~37 μm/s vs. ~46 μm/s) (Fig. 4*B*); meanwhile, the persistence time of microspheres calculated from velocity autocorrelation functions (VACFs) is ~33% lower (~0.08 s vs. ~0.12 s) (Fig. 4*C*). As a result, the diffusivity of microspheres is ~53% lower inside bulges than outside (~84 $\mu m^2/s$ vs. ~178 $\mu m^2/s$) (*Methods*). These results reveal a diffusion-trapping mechanism for microspheres: the diffusivity difference of passive microspheres results in unbalanced particle fluxes into and out of liquid bulges, which in turn would lead to a persistent increase in the surface-packing density of passive particles in liquid bulges until the particle fluxes are balanced.

Taken together, our results based on the motion pattern analysis of passive particles in experiments suggest that pre-existing immotile cells tend to get enriched in liquid bulges via a similar diffusion-trapping mechanism as for passive microspheres, which increases the propensity of biofilm development in liquid bulges. Moreover, as the progenies of immotile cells would be less diffusive in liquid bulges than elsewhere, the enrichment of immotile cells may also trigger positive feedback that expedites colony biofilm development.

Active Brownian Particle Simulation Recapitulates the Essential Dynamics during Bulge Formation. To further understand the dynamics of liquid bulges, we developed an active Brownian particle model (64) (*Methods*). Briefly, rod-shaped cells in the model are represented as self-propelled disk chains moving in a quasi-2D space (65) (Fig. 5*A*). The center positions and orientations of the rod-like particles follow overdamped Langevin dynamics, and the motion is locally coupled due to intercellular steric interactions. In reality, when local activity-induced pressure is beyond a certain threshold set by the surface tension of the swarm fluid film (see the scaling analysis in *Methods*), the swarm fluid film could form stable liquid bulges where cells are able to overlap with each other. In our computational model, this scenario is translated to a key assumption that, when local activity-induced pressure in an area is beyond a certain threshold, the area will be considered as a liquid bulge and the strength of steric interaction in the area will be lowered (Fig. 5 *A*, *Inset* and *Methods*); such a phenomenological treatment accounts for cell–cell overlapping in liquid bulges while avoiding the complication of modeling the geometry of the deformable liquid–air interface (66–68).

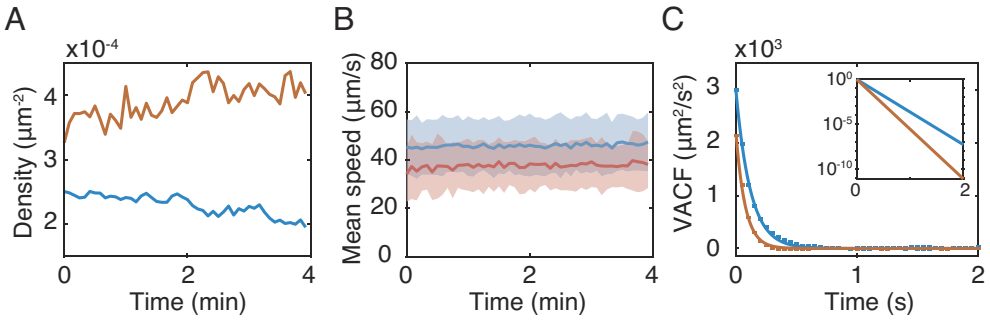

Fig. 4. Enrichment of passive particles toward liquid bulges. (*A*) Surface-packing density of microspheres in bulge area (red) and monolayered regions (blue) plotted against time in a *B. subtilis* swarm. (*B*) Mean speed of microspheres inside (red line) and outside (blue line) liquid bulges plotted against time. The shaded area around each line represents the SD of microsphere speed inside (red) and outside (blue) liquid bulges. Data in panels *A* and *B* was from a representative experiment (three biological replicates). (*C*) VACFs of microsphere that remained inside and outside the liquid bulges computed based on single-particle trajectories. Solid lines are exponential fits to the VACFs [blue: outside liquid bulges, $VACF_{out} \sim \exp(-t/0.12)$, persistence time $\tau_{out} = 0.12 \pm 0.01$ s; red: inside liquid bulges, $VACF_{in} \sim \exp(-t/0.08)$, persistence time $\tau_{in} = 0.08 \pm 0.01$ s). Plotted in the inset are normalized fitted VACFs outside (blue) and inside (red) liquid bulges in a semilogarithmic scale. Error bars represent the SD of N = 3 biological replicates.

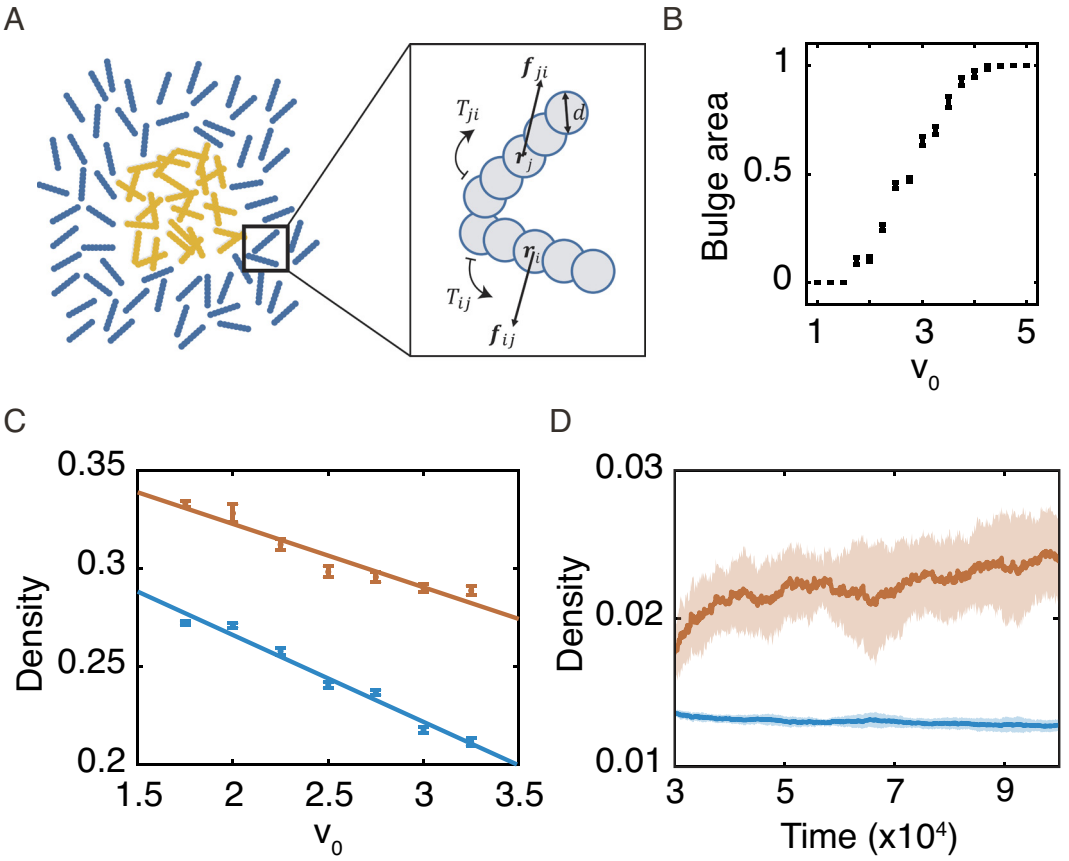

Fig. 5. Active Brownian dynamics simulation recapitulates the speed–density relation and the enrichment of immotile cells in bulge areas. (*A*) Schematic illustration of the active Brownian particle model, which consists of self-propelled rods moving in a quasi-2D space. A bulge area (yellow) develops in the middle of a monolayered region (dark blue). The rectangular box highlights two interacting self-propelled rods moving at a constant active speed v_0. The zoomed-in view shows that the rods *i* and *j* are represented as chains of disk with diameter *d*. The center positions of rods *i* and *j* are r_i and r_j. The interaction forces f_{ij} and f_{ji} (acting on rod *i* and *j*, respectively) changes the center positions of rods and the torques T_{ij} (or T_{ji}) changes the orientation of rods (*Methods*). (*B*) Area fraction of bulges as a function of active speed v_0 ranging from 1 to 5. Error bars represent SD (N = 10 simulation runs). (*C*) Relation between active speed v_0 and normalized particle number density for monolayered regions (blue) and for the coexisting bulges (red) in the simulation. Lines are least-squares linear fits to the data (R^2 = 0.97 for blue line and 0.90 for red line). Error bars represent SD (N = 10 simulation runs). (*D*) Surface-packing density of modeled immotile cells in bulge area (red) and monolayered regions (blue) plotted against time at $v_0 = 2$ in active Brownian particle simulations. Solid lines and shaded areas denote the mean and SD, respectively (N = 16 simulation runs). The simulations started with all the particles being active, and 5% of the particles were set as passive starting at T = 30,000 time steps.

Numerical simulations of the model recapitulate the essential dynamics during bulge formation. With the total cell number held constant, we find that the fraction of bulging area increases with cell motility (Fig. 5*B* and Movie S9), similar to the experimental phenomenon observed during cell speed increase (Fig. 3*A*). Importantly, a negative quasilinear relation between surface-packing cell density and self-propulsion speed (v_0) is reproduced and in agreement with experimental results in Fig. 3*C*, with the ratio between the surface-packing densities inside and outside the bulging area remaining nearly constant regardless of v_0 (Fig. 5*C* and *SI Appendix*, Fig. S9). The consistency between simulation and experiment suggests that the speed–density relation measured in experiment is rooted at the inverse relationship between cell speed and surface-packing cell density for a given bulge-forming threshold of activity-induced pressure (*Methods* and *SI Appendix*, Fig. S10).

Finally, we study the spatial dynamics of immotile cells in the swarm by turning off the activity of a small fraction of cells in the model. In agreement with the experimental result of passive microspheres as shown in Fig. 4, we find that the modeled immotile cells are enriched toward the bulging areas (Fig. 5*D*). During the enrichment of immotile cells, we observe a similar difference in surface-packing density (Fig. 5*D*) and a ~40% difference in diffusivity between immotile cells inside and outside the bulging area (*SI Appendix*, Fig. S11). While immotile cells in a swarm fluid film experience both steric and hydrodynamic interactions with motile cells, our simulation results suggest that purely steric interaction between cells can lead to enrichment or diffusion-trapping of immotile cells in the bulging areas.

Discussion

In this work, we studied the mechanism and the biological function of active interface bulging in *B. subtilis* swarms. Combining multimode imaging, single-cell tracking, and numerical simulations, we showed that active interface bulging promotes biofilm formation at air–solid interface presumably via segregation and enrichment of sessile cells in the bulging area. In particular, the diffusivity of passive particles is ~50% lower inside the bulging area than elsewhere, which enables a diffusion-trapping mechanism and may account for the enrichment of sessile cells. We also uncovered a quasilinear relation between cell speed and surface-packing density that underlies the process of active interface bulging. Guided by the speed–density relation, we demonstrated reversible formation of liquid bulges by manipulating the speed and local density of cells with light. Taken together, our findings reveal a unique physical mechanism of biofilm

formation at air–solid interface and driven self-assembly in active fluids.

The liquid bulges are likely initiated by nonequilibrium density fluctuations (Fig. 3*A*) (58–60), and they develop due to the increase of surface energy supported by activity-induced pressure. The liquid bulges we report here are distinct from those spatial patterns in bacterial swarms driven by nucleation of immotile cells (31) or by a mechanism reminiscent of MIPS (30), although all of these mechanisms yield high-density domains with dynamic and fluctuating boundaries. First of all, liquid bulges consist of almost equally motile cells compared to elsewhere and the liquid bulge formation does not require the presence of pre-existing immotile cells. By contrast, cells in dynamic clusters driven by the nucleation of immotile cells had a much lower speed than those outside the clusters (~80% speed reduction) (31), and the motility of cells in the MIPS-like clusters is also significantly lower than elsewhere due to density-dependent self-trapping (30). Second, liquid bulges have a constant (~20%) difference in surface-packing cell density compared to elsewhere, while the surface-packing density in clusters formed by nucleation of immotile cells or by MIPS-like process continuously increased. Finally, the route of further transition to sessile biofilm state is likely different. In our case, the transition from liquid bulges to sessile biofilm state is suggested to be seeded by the enrichment of sessile cells from surroundings via the unique mechanism of diffusion-trapping. Under our laboratory settings, the MIPS-like clusters were reproduced in swarms with higher cell densities and lower cell speeds, which may fall into the "dry" active matter regime where fluid flows and hydrodynamic interactions became irrelevant (69). However, in our case, the system is a "wet" active matter system, and the hydrodynamic interaction between cells and the deformable air–liquid interface is essential for second-layer formation. This property sets our system apart from the dry active matter systems, including myxobacteria colonies (70) and bacterial colonies grown in hard confinement (e.g., the interstitial space between an agar pad and a glass slide) (66). Note that these bacterial systems are dry only from the active matter perspective. In reality, all living cells must be residing in a fluidic milieu, and the fluidic nature of cell's environment could play important roles even in the absence of hydrodynamic flow. For example, it was recently reported that myxobacteria cells accelerate when meeting the menisci of colloidal particles deposited on an agar surface, suggesting a role of capillary attraction in their gliding motility (71).

Under our experimental conditions (0.6 to 0.8% Luria Broth agar), while the bulge regions transit into biofilm state earlier, other regions of the colony eventually enter the biofilm state as well. We did not see wrinkle structures often observed in *B. subtilis* colony biofilms grown on hard agar surface (e.g., 1.5% agar infused with MSgg medium like that used in ref. 72), presumably due to the difference in surface adhesion (73, 74) or in cell death patterns (72) on substrates with different agar concentrations or different growth media. Nonetheless, we monitored the longer-term evolution of our colony biofilms and found an intriguing role of liquid bulges: A large-scale pattern of parallel ridges with high cell densities emerged in mature colony biofilms, and the position of these ridges lied in between the stripe-shaped bulges that existed earlier in the colony (*SI Appendix*, Fig. S12). After the striped bulges transited into biofilm state, the striped biofilms expanded laterally; the formation of those high-density ridges followed the lateral expansion of the striped biofilms. We speculate that the mechanical stress during lateral expansion of striped biofilms would compress the cell layer in between, which then buckled and rose upward to form the ridges. This phenomenon may deserve further study, as it links interface bulging to the development of large-scale colony biofilm structures.

The phenomenon of active interface bulging and the underlying mechanism reported in this study hold in generic terms, only requiring bacterial motility, a low interface tension, and a high volume density of cells (to enable sufficiently strong active stress and density fluctuations). Given the widespread flagellar motility and surfactant biosynthesis pathways (75) in the microbial world, we expect that active interface bulging is relevant to surface-associated bacterial colonization in many environmental and clinical settings (1, 2), such as on the surface of fresh plant produce (76) and plant roots (54). Motile and sessile populations often coexist in bacterial communities. In complex and fluctuating environments, the transition between the two states may confer certain growth advantage to the population: Cells in sessile state are in general more tolerant to unexpected environmental stresses (77, 78), while cells in motile state can explore more space and proliferate faster. Thus, the motile-to-sessile transition promoted by active interface bulging could potentially serve as a part of a bet-hedging strategy that enhances the adaptability of both in vitro and in vivo surface-associated bacterial communities (24, 42, 43, 79–82).

The ability to control biofilm patterns is essential for engineering bacterial living materials with desired functionalities (32–34). Informed by our study, we envisage that manipulation of cell motility and surface-packing density by either physical stimuli (e.g., light) or genetic control (83) may serve as a general means for biofilm patterning at air–solid interface via liquid bulge formation. Moreover, our results show that the liquid bulges present a physical environment that tends to segregate passive particles from surroundings; the segregation is driven by unbalanced particle fluxes due to the differential diffusivity inside and outside the bulges. As such, manipulating liquid bulge formation enables phase separation or segregation in binary mixtures that consist of passive particles and an active matter bath, providing a unique approach for directed self-assembly of microscopic structures (35, 36) at interfaces.

Methods

The bacterial strains used in this study are listed in *SI Appendix*, Table S2. To prepare bacterial swarms, single-colony isolates were grown overnight (~10 to 12 h) with gyration at 180 rpm in LB broth (1% Bacto tryptone, 0.5% yeast extract, and 0.5% NaCl) at 30 °C. Then, 10 mL swarm agar (0.6% or 0.8% Bacto-Difco agar infused with 1% Bacto tryptone, 0.5% Yeast Extract, and 0.5% NaCl) was melted in a microwave oven and poured to a polystyrene Petri dish (90 mm diameter, 15 mm height). The plates were placed inside a Plexiglas box with the lid off for 10 min. After that, 1 to 2.5 μL diluted overnight culture (OD_{600} ~ 1) were inoculated at 1.5 cm from the edge of the plate. Swarm plates were incubated at 30 °C and ~50% relative humidity for 6 to 7 h before imaging. The wetness of agar surface is a key factor for the formation of liquid bulges. For characterization of cell density, the membrane stain FM4-64 (Life Technologies, Cat. No. T13320) dissolved in deionized water was added at a final concentration of 1.0 μg/mL into the molten agar before it was poured into Petri dishes. The detailed methods of imaging, image processing, data analysis, and Active Brownian Dynamics modeling are described in *SI Appendix, SI Methods*.

Data, Materials, and Software Availability. All study data are included in the article and/or supporting information.

ACKNOWLEDGMENTS. We thank Harald Putzer and Yunrong Chai for their kind gifts of bacterial strains; Wenlong Zuo for providing the custom-written single-cell tracking program; Lei Xu for assistance with darkfield imaging; and Munehiro Asally and Marco Polin for helpful discussions. This work was supported by Research Grants Council of Hong Kong SAR (RGC Ref. No. 14309023, 14307822, 14307821, RFS2021-4S04, and CUHK Direct Grants; to Y.W.); NIH of United States (R35 GM131783 to D.B.K); and National Natural Science Foundation of China (NSFC No. 32101002 to Y.L. and 31971182 to Y.W.).

1. L. Hall-Stoodley, J. W. Costerton, P. Stoodley, Bacterial biofilms: From the natural environment to infectious diseases. *Nat. Rev. Microbiol.* **2**, 95–108 (2004).
2. D. López, H. Vlamakis, R. Kolter, Biofilms. *Cold Spring Harb. Perspect. Biol.* **2**, a000398 (2010).
3. R. M. Harshey, Bacterial motility on a surface: Many ways to a common goal. *Annu. Rev. Microbiol.* **57**, 249–273 (2003).
4. D. B. Kearns, A field guide to bacterial swarming motility. *Nat. Rev. Microbiol.* **8**, 634–644 (2010).
5. S. S. Branda, J. E. González-Pastor, S. Ben-Yehuda, R. Losick, R. Kolter, Fruiting body formation by Bacillus subtilis. *Proc. Natl. Acad. Sci. U.S.A.* **98**, 11621–11626 (2001).
6. J.-P. Motta, J. L. Wallace, A. G. Buret, C. Deraison, N. Vergnolle, Gastrointestinal biofilms in health and disease. *Nat. Rev. Gastroenterol. Hepatol.* **18**, 314–334 (2021).
7. L. D. Renner, D. B. Weibel, Physicochemical regulation of biofilm formation. *MRS Bull.* **36**, 347–355 (2011).
8. A. Persat *et al.*, The mechanical world of bacteria. *Cell* **161**, 988–997 (2015).
9. G. A. O'Toole, G. C. Wong, Sensational biofilms: Surface sensing in bacteria. *Curr. Opin. Microbiol.* **30**, 139–146 (2016).
10. G. C. L. Wong *et al.*, Roadmap on emerging concepts in the physical biology of bacterial biofilms: From surface sensing to community formation. *Phys. Biol.* **18**, 051501 (2021).
11. H. Xu, M. R. Nejad, J. M. Yeomans, Y. Wu, Geometrical control of interface patterning underlies active matter invasion. *Proc. Natl. Acad. Sci. U.S.A.* **120**, e2219708120 (2023).
12. C. Fei *et al.*, Nonuniform growth and surface friction determine bacterial biofilm morphology on soft substrates. *Proc. Natl. Acad. Sci. U.S.A.* **117**, 7622–7632 (2020).
13. J. Nijjer *et al.*, Mechanical forces drive a reorientation cascade leading to biofilm self-patterning. *Nat. Commun.* **12**, 6632 (2021).
14. T. E. Angelini, M. Roper, R. Kolter, D. A. Weitz, M. P. Brenner, *Bacillus subtilis* spreads by surfing on waves of surfactant. *Proc. Natl. Acad. Sci. U.S.A.* **106**, 18109–18113 (2009).
15. M. Fauvart *et al.*, Surface tension gradient control of bacterial swarming in colonies of Pseudomonas aeruginosa. *Soft Matter* **8**, 70–76 (2012).
16. H. Du *et al.*, High density waves of the Bacterium Pseudomonas aeruginosa in propagating swarms result in efficient colonization of surfaces. *Biophys. J.* **103**, 601–609 (2012).
17. S. Trinschek, K. John, U. Thiele, Modelling of surfactant-driven front instabilities in spreading bacterial colonies. *Soft Matter* **14**, 4464–4476 (2018).
18. B. Rhodeland, K. Hoeger, T. Ursell, Bacterial surface motility is modulated by colony-scale flow and granular jamming. *J. R Soc. Interface* **17**, 20200147 (2020).
19. H. Ma, J. Bell, W. Chen, S. Mani, J. X. Tang, An expanding bacterial colony forms a depletion zone with growing droplets. *Soft Matter* **17**, 2315–2326 (2021).
20. Y. Li *et al.*, Self-organized canals enable long-range directed material transport in bacterial communities. *Elife* **11**, e79780 (2022).
21. N. Verstraeten *et al.*, Living on a surface: Swarming and biofilm formation. *Trends Microbiol.* **16**, 496–506 (2008).
22. R. Belas, Biofilms, flagella, and mechanosensing of surfaces by bacteria. *Trends Microbiol.* **22**, 517–527 (2014).
23. D. B. Kearns, R. Losick, Cell population heterogeneity during growth of Bacillus subtilis. *Genes Dev.* **19**, 3083–3094 (2005).
24. H. Jeckel *et al.*, Simultaneous spatiotemporal transcriptomics and microscopy of Bacillus subtilis swarm development reveal cooperation across generations. *Nat. Microbiol.* **8**, 2378–2391 (2023).
25. L. McCarter, M. Hilmen, M. Silverman, Flagellar dynamometer controls swarmer cell differentiation of *V. parahaemolyticus*. *Cell* **54**, 345–351 (1988).
26. A. Persat, F. Inclan Yuki, N. Engel Joanne, A. Stone Howard, Z. Gitai, Type IV pili mechanochemically regulate virulence factors in Pseudomonas aeruginosa. *Proc. Natl. Acad. Sci. U.S.A.* **112**, 7563–7568 (2015).
27. C.K. Ellison *et al.*, Obstruction of pilus retraction stimulates bacterial surface sensing. *Science* **358**, 535–538 (2017).
28. K. Otto, T. J. Silhavy, Surface sensing and adhesion of Escherichia coli controlled by the Cpx-signaling pathway. *Proc. Natl. Acad. Sci. U.S.A.* **99**, 2287–2292 (2002).
29. N. Majdalani, S. Gottesman, The Rcs phosphorelay: A complex signal transduction system. *Annu. Rev. Microbiol.* **59**, 379–405 (2005).
30. I. Grobas, M. Polin, M. Asally, Swarming bacteria undergo localized dynamic phase transition to form stress-induced biofilms. *Elife* **10**, e62632 (2021).
31. M. Worlitzer Vasco *et al.*, Biophysical aspects underlying the swarm to biofilm transition. *Sci. Adv.* **8**, eabn8152 (2022).
32. A. Rodrigo-Navarro, S. Sankaran, M. J. Dalby, A. del Campo, M. Salmeron-Sanchez, Engineered living biomaterials. *Nat. Rev. Mater.* **6**, 1175–1190 (2021).
33. X. Jin, H. Riedel-Kruse Ingmar, Biofilm Lithography enables high-resolution cell patterning via optogenetic adhesin expression. *Proc. Natl. Acad. Sci. U.S.A.* **115**, 3698–3703 (2018).
34. Y. Wang *et al.*, Living materials fabricated via gradient mineralization of light-inducible biofilms. *Nat. Chem. Biol.* **17**, 351–359 (2021).
35. J. Stenhammar, R. Wittkowski, D. Marenduzzo, M. E. Cates, Activity-induced phase separation and self-assembly in mixtures of active and passive particles. *Phys. Rev. Lett.* **114**, 018301 (2015).
36. D. P. Singh, U. Choudhury, P. Fischer, A. G. Mark, Non-equilibrium assembly of light-activated colloidal mixtures. *Adv. Mater.* **29**, 1701328 (2017).
37. J. Arlt, V. A. Martinez, A. Dawson, T. Pilizota, W. C. K. Poon, Painting with light-powered bacteria. *Nat. Commun.* **9**, 768 (2018).
38. G. Frangipane *et al.*, Dynamic density shaping of photokinetic E. coli. *Elife* **7**, e36608 (2018).
39. R. Zhang, L. Turner, H. C. Berg, The upper surface of an *Escherichia coli* swarm is stationary. *Proc. Natl. Acad. Sci. U.S.A.* **107**, 288–290 (2010).
40. Y. Wu, H. C. Berg, Water reservoir maintained by cell growth fuels the spreading of a bacterial swarm. *Proc. Natl. Acad. Sci. U.S.A.* **109**, 4128–4133 (2012).
41. M. E. Cates, D. Marenduzzo, I. Pagonabarraga, J. Tailleur, Arrested phase separation in reproducing bacteria creates a generic route to pattern formation. *Proc. Natl. Acad. Sci. U.S.A.* **107**, 11715–11720 (2010).
42. K. Hamze *et al.*, Single-cell analysis in situ in a Bacillus subtilis swarming community identifies distinct spatially separated subpopulations differentially expressing hag (flagellin), including specialized swarmers. *Microbiology* **157**, 2456–2469 (2011).
43. L. Hamouche *et al.*, Bacillus subtilis swarmer cells lead the swarm, multiply, and generate a trail of quiescent descendants. *mBio* **8**, e02102–16 (2017).
44. S. B. Guttenplan, D. B. Kearns, Regulation of flagellar motility during biofilm formation. *FEMS Microbiol. Rev.* **37**, 849–871 (2013).
45. N. D. Lord *et al.*, Stochastic antagonism between two proteins governs a bacterial cell fate switch. *Science* **366**, 116–120 (2019).
46. T. M. Norman, N. D. Lord, J. Paulsson, R. Losick, Memory and modularity in cell-fate decision making. *Nature* **503**, 481–486 (2013).
47. D. B. Kearns, F. Chu, S. S. Branda, R. Kolter, R. Losick, A master regulator for biofilm formation by Bacillus subtilis. *Mol. Microbiol.* **55**, 739–749 (2005).
48. Y. Chai, F. Chu, R. Kolter, R. Losick, Bistability and biofilm formation in Bacillus subtilis. *Mol. Microbiol.* **67**, 254–263 (2008).
49. H. Vlamakis, C. Aguilar, R. Losick, R. Kolter, Control of cell fate by the formation of an architecturally complex bacterial community. *Genes. Dev.* **22**, 945–953 (2008).
50. D. Romero, H. Vlamakis, R. Losick, R. Kolter, An accessory protein required for anchoring and assembly of amyloid fibres in B. subtilis biofilms. *Mol. Microbiol.* **80**, 1155–1168 (2011).
51. J. van Gestel, H. Vlamakis, R. Kolter, New tools for comparing microscopy images: Quantitative analysis of cell types in Bacillus subtilis. *J. Bacteriol.* **197**, 699–709 (2015).
52. H. Vlamakis, Y. Chai, P. Beauregard, R. Losick, R. Kolter, Sticking together: Building a biofilm the Bacillus subtilis way. *Nat. Rev. Microbiol.* **11**, 157–168 (2013).
53. H.-C. Flemming, J. Wingender, The biofilm matrix. *Nat. Rev. Microbiol.* **8**, 623–633 (2010).
54. P. B. Beauregard, Y. Chai, H. Vlamakis, R. Losick, R. Kolter, *Bacillus subtilis* biofilm induction by plant polysaccharides. *Proc. Natl. Acad. Sci. U.S.A.* **110**, E1621–E1630 (2013).
55. R. Bleich, J. D. Watrous, P. C. Dorrestein, A. A. Bowers, E. A. Shank, Thiopeptide antibiotics stimulate biofilm formation in Bacillus subtilis. *Proc. Natl. Acad. Sci. U.S.A.* **112**, 3086–3091 (2015).
56. T. Kimura, K. Kobayashi, Role of glutamate synthase in biofilm formation by Bacillus subtilis. *J. Bacteriol.* **202**, e00120-20 (2020), 10.1128/jb.00120-00120.
57. J. Pogliano *et al.*, A vital stain for studying membrane dynamics in bacteria: A novel mechanism controlling septation during Bacillus subtilis sporulation. *Mol. Microbiol.* **31**, 1149–1159 (1999).
58. F. Peruani, A. Deutsch, M. Bär, Nonequilibrium clustering of self-propelled rods. *Phys. Rev. E* **74**, 030904 (2006).
59. V. Narayan, S. Ramaswamy, N. Menon, Long-lived giant number fluctuations in a swarming granular nematic. *Science* **317**, 105–108 (2007).
60. H. P. Zhang, A. Be'er, E.-L. Florin, H. L. Swinney, Collective motion and density fluctuations in bacterial colonies. *Proc. Natl. Acad. Sci. U.S.A.* **107**, 13626–13630 (2010).
61. B. L. Taylor, D. E. Koshland, Intrinsic and extrinsic light responses of Salmonella typhimurium and Escherichia coli. *J. Bacteriol.* **123**, 557–569 (1975).
62. J. Tailleur, M. E. Cates, Statistical mechanics of interacting run-and-tumble bacteria. *Phys. Rev. Lett.* **100**, 218103 (2008).
63. J. Arlt, V. A. Martinez, A. Dawson, T. Pilizota, W. C. K. Poon, Dynamics-dependent density distribution in active suspensions. *Nat. Commun.* **10**, 2321 (2019).
64. P. Romanczuk, M. Bär, W. Ebeling, B. Lindner, L. Schimansky-Geier, Active Brownian particles. *Eur. Phys. J. Spl. Topics* **202**, 1–162 (2012).
65. S. Weitz, A. Deutsch, F. Peruani, Self-propelled rods exhibit a phase-separated state characterized by the presence of active stresses and the ejection of polar clusters. *Phys. Rev. E* **92**, 012322 (2015).
66. S. C. Takatori, K. K. Mandadapu, Motility-induced buckling and glassy dynamics regulate three-dimensional transitions of bacterial monolayers. arXiv [Preprint] (2020). https://doi.org/10.48550/arXiv.2003.05618 (Accessed 12 March 2020).
67. L. J. Ruske, J. M. Yeomans, Morphology of active deformable 3D droplets. *Phys. Rev. X* **11**, 021001 (2021).
68. R. Alert, Fingering instability of active nematic droplets. *J. Phys. A Math. Theor.* **55**, 234009 (2022).
69. M. C. Marchetti *et al.*, Hydrodynamics of soft active matter. *Rev. Mod. Phys.* **85**, 1143–1189 (2013).
70. K. Copenhagen, R. Alert, N. S. Wingreen, J. W. Shaevitz, Topological defects promote layer formation in Myxococcus xanthus colonies. *Nat. Phys.* **17**, 211–215 (2021).
71. C. H. Ramos *et al.*, The environment topography alters the way to multicellularity in *Myxococcus xanthus*. *Sci. Adv.* **7**, eabh2278 (2021).
72. M. Asally *et al.*, Localized cell death focuses mechanical forces during 3D patterning in a biofilm. *Proc. Natl. Acad. Sci. U.S.A.* **109**, 18891–18896 (2012).
73. J. Yan *et al.*, Mechanical instability and interfacial energy drive biofilm morphogenesis. *Elife* **8**, e43920 (2019).
74. S. Geisel, E. Secchi, J. Vermant, The role of surface adhesion on the macroscopic wrinkling of biofilms. *Elife* **11**, e76027 (2022).
75. E. Z. Ron, E. Rosenberg, Natural roles of biosurfactants. *Environ. Microbiol.* **3**, 229–236 (2001).
76. S. Yaron, U. Römling, Biofilm formation by enteric pathogens and its role in plant colonization and persistence. *Microb. Biotechnol.* **7**, 496–516 (2014).
77. T.-F.C. Mah, G. A. O'Toole, Mechanisms of biofilm resistance to antimicrobial agents. *Trends Microbiol.* **9**, 34–39 (2001).
78. N. Hoiby, T. Bjarnsholt, M. Givskov, S. Molin, O. Ciofu, Antibiotic resistance of bacterial biofilms. *Int. J. Antimicrob. Agents* **35**, 322–332 (2010).
79. J. van Gestel, H. Vlamakis, R. Kolter, Division of labor in biofilms: The ecology of cell differentiation. *Microbiol. Spectrum* **3**, Mb-0002-2014 (2015).
80. A. Dragoš *et al.*, Division of labor during biofilm matrix production. *Curr. Biol.* **28**, 1903–1913.e5 (2018).
81. M. Martin *et al.*, Cheaters shape the evolution of phenotypic heterogeneity in Bacillus subtilis biofilms. *ISME J.* **14**, 2302–2312 (2020).
82. S. Arnaouteli, N. C. Bamford, N. R. Stanley-Wall, Á. T. Kovács, Bacillus subtilis biofilm formation and social interactions. *Nat. Rev. Microbiol.* **19**, 600–614 (2021).
83. A. I. Curatolo *et al.*, Cooperative pattern formation in multi-component bacterial systems through reciprocal motility regulation. *Nat. Phys.* **16**, 1152–1157 (2020).